Article

Circular Array of Magnetic Sensors for Current Measurement: Analysis for Error Caused by Position of Conductor

Hao Yu [1], Zheng Qian [1,*], Huayi Liu[1] and Jiaqi Qu[1]

[1] School of Instrumentation Science and Opto-electronics Engineering, Beihang University, Beijing 100191, China; E-Mail: yuhaoby@buaa.edu.cn (H.Y.); liuhy_one@163.com (H.L.); qujiaqi@buaa.edu.cn (J.Q.)

* Correspondence: qianzheng@buaa.edu.cn; Tel.: +86-010-8233-9267

Abstract: This paper analyzes the measurement error, caused by the position of the current-carrying conductor, of circular array of magnetic sensors for current measurement. The circular array of magnetic sensors is an effective approach for AC or DC non-contact measurement, as its low cost, large linear range, wide bandwidth, light weight and low noise. Especially it has claimed that such structure has the excellent reduction ability for the errors caused by the position of the current-carrying conductor, crosstalk current interference, shape of the conduction cross section and the earth magnetic field. However, the positions of the current-carrying conductor, including un-center and un-perpendicularity, has not analyzed in detail until now. In this paper, the theoretical analysis has been proposed based on vector inner and exterior product. In the presented mathematical model of relative error, the un-center offset distance, the un-perpendicular angle, the radius of the circle and the number of the magnetic sensor are expressed in one equation. The comparison of the relative error caused by the position of the current-carrying conductor between four and eight sensors is conducted. The Tunnel Magnetoresistance (TMR) sensors are used in the experimental prototype to verify the mathematical model. The analysis results can be the reference to design the detail of circular array of magnetic sensors for current measurement in practical situation.

Keywords: circular array; current measurement; un-center; un-perpendicular; Tunnel Magnetoresistance sensors

1. Introduction

Magnetic sensors have been widely used for non-contact current measurement, such as Hall sensor, fluxgate sensor, Anisotropic Magnetoresistance (AMR) sensor, Giant Magnetoresistance (GMR) sensor [1] and Tunnel Magnetoresistance (TMR) sensor. In order to improve the measurement accuracy, the structure based on circular array of magnetic sensors has being frequently studied during the past two decades [2–8]. Distinguishing with other structures, such as open-loop or close-loop with magnetic cores, current transformers, etc. [9], the circular array of magnetic sensors is considered a effective scheme to achieve low cost, large linear range, wide frequency bandwidth [10–12], light weight and high reliability. Especially, the circular array of magnetic sensor can detect both DC and high frequency AC, compared to Rogowski coil [13], which can only measure high frequency current. However, measurement accuracy of such structure is mainly suffering with the error caused by position of the current-carrying conductor and the crosstalk current interference. Much research has focused on the relationship between the error reduction ability and the parameters of the circular array of magnetic sensors.

The installation position offset of the current-carrying conductor also influence the accuracy of magnetic sensor circular array, including wire un-center and un-perpendicularity. In [5], the relative measurement error dependence on the displacement of the conductor from the center of the circle has

Preprints (www.preprints.org) | NOT PEER-REVIEWED | Posted: 29 January 2018 doi:10.20944/preprints201801.0272.v1

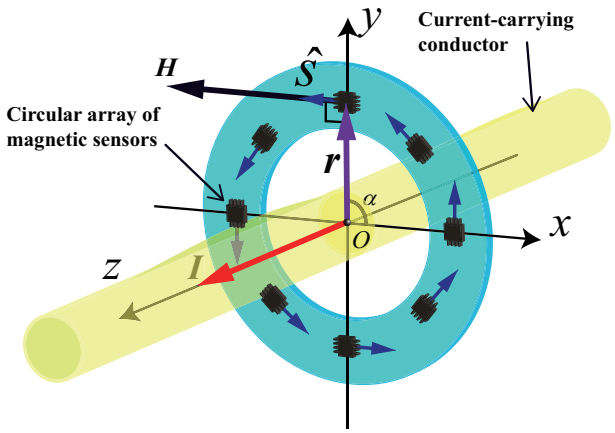

Figure 1. Basic theory of the circular array of eight magnetic sensors.

been discussed, the displacement angles between the first sensor to x-axis (α_0) also considered in the theoretical analysis. As different from other works, AMR sensors have been applied.

The crosstalk current effect is considered as one of the important factors that limit the measurement accuracy, which has been generally discussed [4,6]. A algorithm base on Discrete Fourier Transform (DFT) to improve the crosstalk reduction has been proposed, which can be realized on DSP or other microcontroller [3]. In their work, circular array of eight Hall sensors was used to verify the efficiency of the crosstalk error reduction algorithm. Then, Roland Weiss *et al*.[6] improved the modeling and the experimental setup of above method and verified with six fluxgate sensors. The effect of different displacement angles between the first sensor to x-axis (α_0) has been discussed. They also analyzed the effect of the geometry of different flat conductors in another work [7], and achieved the current errors of less than 1.5%.

However, although the measurement caused by un-center has been discuss, no researcher has addressed the problem about the conductor un-perpendicularity until now. Unfortunately, the conductor un-perpendicularity is non-ignorable factor especially in the situation the conductor is soft wire, and usually it may combined with the un-center offset. Based on above issues, this paper used the inner and exterior product in vector space, analyzed the error caused by the current-carrying conductor position conveniently, includes un-center and un-perpendicularity. The experiment based on high performance commercial TMR sensors has been conducted to verify the theoretical model. The combination effect is also discussed in our work. Finally, the allowable range of un-center offset and un-perpendicularity angle can be given by the mathematic model.

2. Mathematical Background

The structure of circular array of magnetic sensors are shown in Figure 1. Eight or other number magnetic sensors uniformly arranged in a circular with a radius of r. The sensors can be installed on a printed circuit board (PCB), and the sensitivity directions are always perpendicular to $\boldsymbol{r}$, the vector from the center to the sensor sensitivity point. The current-carrying conductor, which is strictly straight and has a proximate infinite length, crosses from the center of the circle. In three dimensional Cartesian coordinate system, according to Biot-Savart law [14], the output signal of an individual magnetic sensor, V, can be expressed by

$$V = k_s(\boldsymbol{H} \cdot \hat{\boldsymbol{s}}) = k_s \frac{\boldsymbol{I} \times \boldsymbol{r}}{2\pi r^2} \cdot \hat{\boldsymbol{s}} \tag{1}$$

Preprints (www.preprints.org) | NOT PEER-REVIEWED | Posted: 29 January 2018 doi:10.20944/preprints201801.0272.v1

where, k_s is the sensitivity parameter of magnetic sensors (assuming the sensors are linear and totally accordance), $\boldsymbol{H}$ is the vector of magnetic field generated by the current-carrying conductor, $\boldsymbol{I}$ is the current vector in the conductor, $\hat{\boldsymbol{s}}$ is the unit vector ($|\hat{\boldsymbol{s}}| = 1$) of sensitivity direction of magnetic sensor. In (1), according to the definition of exterior product, $\boldsymbol{I} \times \boldsymbol{r}$ means the result is a vector which is both perpendicular to $\boldsymbol{I}$ and $\boldsymbol{r}$, and follows the right-hand rule. At the same time, according to the definition of inner product, $\boldsymbol{H} \cdot \hat{\boldsymbol{s}}$ means the result is the projection value of the vector $\boldsymbol{H}$ on the direction $\hat{\boldsymbol{s}}$, it represents the output of magnetic sensor only relates with the magnetic field along the sensitivity direction.

In a circular array constructed by N magnetic sensors, the mean value of the sensor outputs can be expressed as

$$V_{mean} = \frac{1}{N}\sum_{n=1}^{N} V^{(n)} = \frac{k_s}{N}\sum_{n=1}^{N}(\boldsymbol{H}^{(n)} \cdot \hat{\boldsymbol{s}}^{(n)}) = \frac{k_s}{N}\sum_{n=1}^{N}\frac{\boldsymbol{I} \times \boldsymbol{r}^{(n)}}{2\pi(r^{(n)})^2} \cdot \hat{\boldsymbol{s}}^{(n)} \tag{2}$$

where, the superscript (n) represents the nth sensor parameters, for instance, $\hat{\boldsymbol{s}}^{(1)}$ is the sensitivity direction of the first magnetic sensor. For V_{mean} can be easily measured and calculated, k_s can be a constant after calibration, the measured $\boldsymbol{I}$ is the only unknown quantity in (2). If the current-carrying conductor offsets from the center or not be perpendicular to the circle plane, $r^{(n)} = |\boldsymbol{r}^{(n)}|$ will have different values, otherwise, they will be equal ($r^{(n)} = r$) in ideal condition. Therefore, the calculated current value, I_{cal}, of the under measured current, can be calculated by

$$I_{cal} = \frac{2\pi r V_{mean}}{k_s} \tag{3}$$

and relative measurement error is

$$\varepsilon = \frac{|I_{cal} - I|}{I} \times 100\% \tag{4}$$

3. The Error Analysis

3.1. The mathematical model of the errors from the un-center and un-perpendicularity

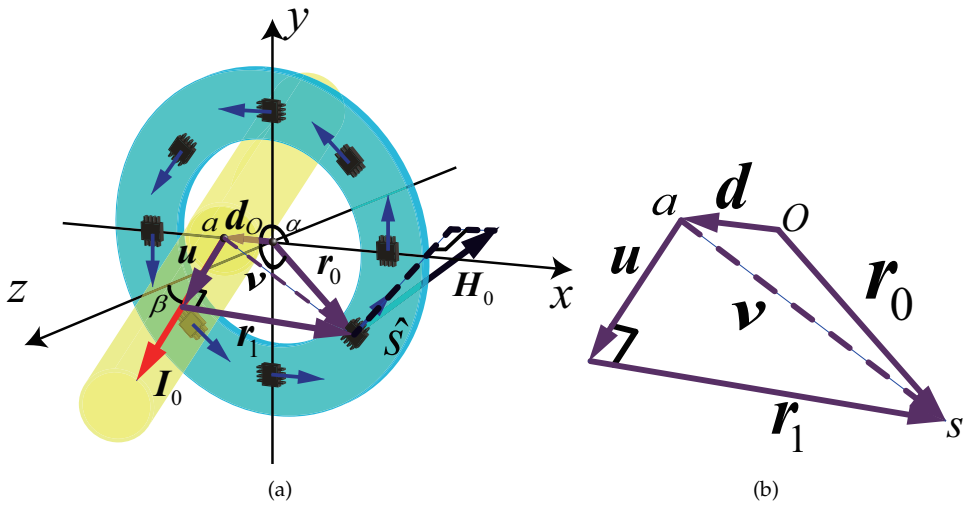

Figure 2. The error caused by the current-carrying conductor position: (**a**) schematic of Un-center and un-perpendicularity; (**b**) The relationship of the key position vectors

Preprints (www.preprints.org) | NOT PEER-REVIEWED | Posted: 29 January 2018 doi:10.20944/preprints201801.0272.v1

Un-center and un-perpendicularity of the current-carrying conductor may coexist in practical situation. The modelling method introduced in the mathematical background is useful to analysis the measurement errors caused by these factors. Figure 2 shows the magnetic filed generated by the under measured current $\boldsymbol{I}_0$, which crosses the offset point a from the center, and be un-perpendicular to the circle plane. The parameter d presents the offset distance from the circle center and β presents the un-perpendicularity angle from z-axis, where $d < r_0$ and $0 < \beta < \pi/2$. The definitions and values of the vectors in Figure 2 are list in Table 1. Note that the superscript (n) is not used for the moment.

Table 1. Parameters and vectors in Figure 2

Vector	Norm	Value	Definition
$\boldsymbol{I_0}$	I_0	$I_0(sin\beta, 0, cos\beta)^T$	Under measured current
$\boldsymbol{d}$	d	$(d, 0, 0)^T$	Offset vector from the center
$\boldsymbol{r}_0$	r_0	$r_0(cos\alpha, sin\alpha, 0)^T$*	Position vector from O to sensor
$\boldsymbol{v}$	v	$\boldsymbol{r_0} - \boldsymbol{d}$	Position vector from point a to sensor
$\boldsymbol{r}_1$	r_1	$\boldsymbol{v} - \boldsymbol{u}$	Position vector from $\boldsymbol{I}_0$ to sensor
$\boldsymbol{u}$	u	see (5)	Position vector from O to $\boldsymbol{r}_1$
$\hat{\boldsymbol{s}}$**	1	$(-sin\alpha, cos\alpha, 0)^T$	Sensitivity direction of sensor

* α *is the angle between* x*-axie and* $\boldsymbol{r}_0$
** $\hat{\boldsymbol{s}}$ *is perpendicular to* $\boldsymbol{r}_0$

Additionally, the norn of $\boldsymbol{u}$ is the projection of $\boldsymbol{v}$ on $\boldsymbol{I}_0$, according to the definition of vector inner product, $\boldsymbol{u}$ can be calculated by

$$\boldsymbol{u} = |\boldsymbol{u}|\hat{\boldsymbol{I}}_0 = \boldsymbol{v} \cdot \hat{\boldsymbol{I}}_0 \cdot \hat{\boldsymbol{I}}_0 = \begin{bmatrix} sin^2\beta(r_0 cos\alpha - d) \\ 0 \\ sin\beta cos\beta(r_0 cos\alpha - d) \end{bmatrix} \tag{5}$$

From the vectors relationship schematic diagram in Figure 2, the vector from $\boldsymbol{I}_0$ to the sensor can be calculated by

$$\boldsymbol{r}_1 = \boldsymbol{r}_0 - \boldsymbol{d} - \boldsymbol{u} = \begin{bmatrix} cos^2\beta(r_0 cos\alpha - d) \\ r_0 sin\alpha \\ sin\beta cos\beta(d - r_0 cos\alpha) \end{bmatrix} \tag{6}$$

According to (2), the mean value of output signal of sensors can be straightly written as

$$\begin{aligned} V_{mean} &= \frac{k_s I_{cal}}{2\pi r_0} = \frac{1}{N}\sum_{n=1}^{N} V^{(n)} = \frac{k_s}{N}\sum_{n=1}^{N}(\boldsymbol{H}_0^{(n)} \cdot \hat{\boldsymbol{s}}^{(n)}) = \frac{k_s}{N}\sum_{n=1}^{N}\frac{\boldsymbol{I}_0 \times \boldsymbol{r}_1^{(n)}}{2\pi(r_1^{(n)})^2} \cdot \hat{\boldsymbol{s}}^{(n)} \\ &= I_0\frac{k_s}{2\pi N}\sum_{n=1}^{N}\frac{cos\beta(r_0 - d cos\alpha^{(n)})}{cos^2\beta(r_0 cos\alpha^{(n)} - d)^2 + r_0^2 sin^2\alpha^{(n)}} \end{aligned} \tag{7}$$

where $\alpha^{(n)}$ is the angle between the nth sensor position vector $\boldsymbol{r}_0^{(n)}$ and $+x$-axis, which is expressed by

$$\alpha^{(n)} = \frac{2\pi n}{N} + \alpha_0 \quad (n = 0, 1, ..., N-1) \tag{8}$$

Preprints (www.preprints.org) | NOT PEER-REVIEWED | Posted: 29 January 2018 doi:10.20944/preprints201801.0272.v1

where α_0 is the offset angle between magnetic sensor array and the $+x$-axis, which is a non-negligible parameter effecting the measurement error refer to [5] and [7]. We will analyze the effect of α_0 later.

The calculated current I_{cal} in (7) is the calculated current by the circular array of magnetic sensors, which can be written as

$$I_{cal} = I_0 \frac{r_0}{N} \sum_{n=1}^{N} \frac{cos\beta(r_0 - dcos\alpha^{(n)})}{cos^2\beta(r_0 cos\alpha^{(n)} - d)^2 + r_0^2 sin^2\alpha^{(n)}} = I_0\Delta \tag{9}$$

where Δ is the key part of which coursing the measurement error and it can be proved that,

$$\lim_{N\to+\infty} \Delta = 1, \tag{10}$$

Therefore, equation (10) leads I_{cal} being approximate equal to actual under measured current I_0, which theoretically proves that, the sum of the output of the circular array is an approximation of the Ampere's circulation, when $N \to +\infty$. According to the method proposed by Weiss *et al*. [6], the relative error ε / I_0 is used to present the effect caused by d and β, which actually is the Δ in our equation(9). Therefore, the relative measurement error caused by d and β is

$$\varepsilon_{d\beta} = \frac{I_{cal} - I_0}{I_0} \times 100\% = \Delta - 1 = \frac{r_0}{N} \sum_{n=1}^{N} \frac{cos\beta(r_0 - dcos\alpha^{(n)})}{cos^2\beta(r_0 cos\alpha^{(n)} - d)^2 + r_0^2 sin^2\alpha^{(n)}} - 1 \tag{11}$$

Finally, for convenience, the situation of un-center and un-perpendicularity are discussed respectively. For $\beta = 0$, the relative measurement error caused by d is

$$\varepsilon_d = \frac{r_0}{N} \sum_{n=1}^{N} \frac{r_0 - dcos\alpha^{(n)}}{r_0^2 + d^2 - 2r_0 dcos\alpha^{(n)}} - 1 \tag{12}$$

and for $d = 0$, the relative measurement error caused by β is

$$\varepsilon_\beta = \frac{1}{N} \sum_{n=1}^{N} \frac{cos\beta}{(1 - cos^2\alpha^{(n)} sin^2\beta)} - 1 \tag{13}$$

Note that, r_0 does not exist in ε_β, meaning that the ε_β has no relationship with r_0.

3.2. Analysis for the effect of displacement angles of the sensors array

To analyze the effect of the displacement angles of the sensors array α_0 on ε_d and ε_β, we calculated the $\varepsilon_{d\beta}$ with the sensor number $N = 4$ and $N = 8$. In our case, $r_0 = 40$ mm. In Figure 3(a) and Figure 3(b), it can be seen, for d ranges from 0 mm to 23 mm, the relative error ε_d reaches max point when $\alpha_0 = 2\pi n/N$, and min point approximately when $\alpha_0 = \pi(2n+1)/2N$. Note that, for $d = 23$ mm, the maximum ε_d reduces from 12.27% to 1.21% while N increase from 4 to 8. The same above results can also be find in Figure 3(c) and 3(d), while $d = 0$, β ranges from 0° to 60°.

Based on above analysis, it can be concluded that the change of α_0 can reduce the relative error effectively. The relative error may be particularly reduced to small level that can be ignored. However, unfortunately for practical situation, the position of the conductor is usually uncertain, so is the α_0. Therefore, we keep the $\alpha_0 = 0^\circ$ in our rest analysis, to study the maximum effect on measurement accuracy of the position error of the current-carrying conductor.

Preprints (www.preprints.org) | NOT PEER-REVIEWED | Posted: 29 January 2018 doi:10.20944/preprints201801.0272.v1

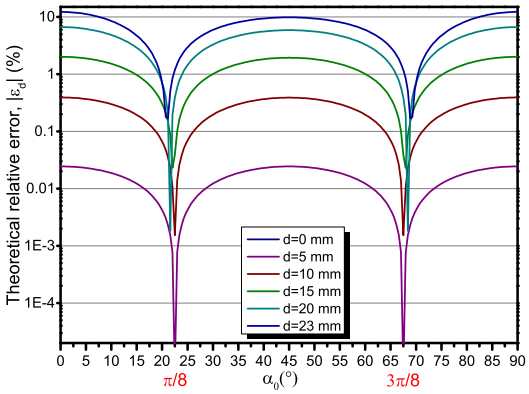

(a) α_0 and d, with $N = 4$, $\beta = 0°$.

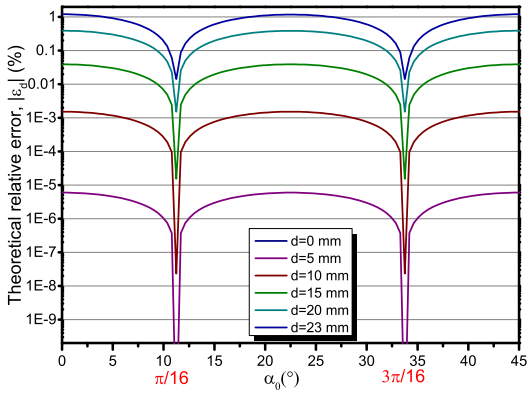

(b) α_0 and d, with $N = 8$, $\beta = 0°$.

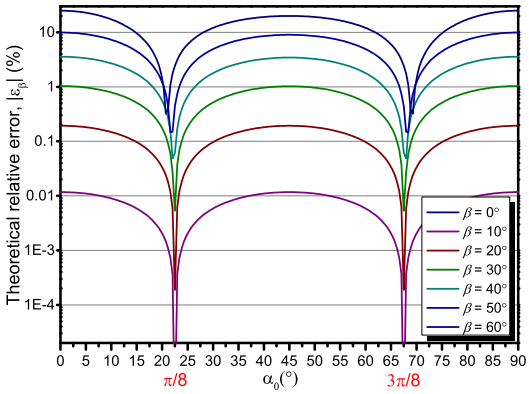

(c) α_0 and β, with $N = 4$, $d = 0$.

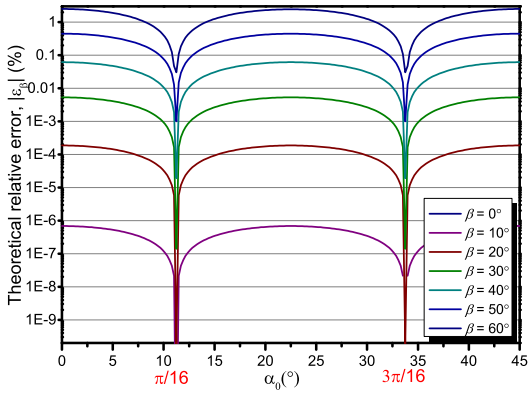

(d) α_0 and β, with $N = 8$, $d = 0$.

Figure 3. The theoretical relative error analysis depend on α_0, β and d, with $r_0 = 40$ mm.

Preprints (www.preprints.org) | NOT PEER-REVIEWED | Posted: 29 January 2018 doi:10.20944/preprints201801.0272.v1

3.3. Analysis for the effect of un-center and un-perpendicularity

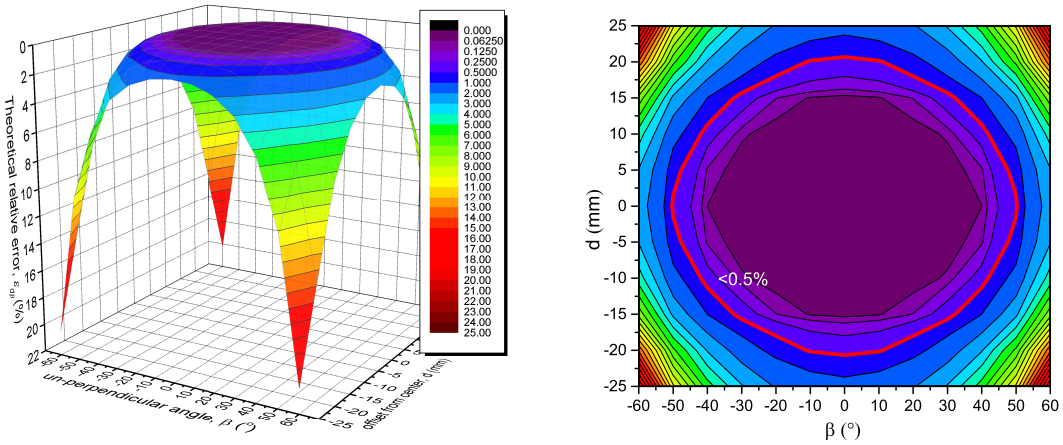

(a) (b)

Figure 4. The theoretical relative error depend on d and β, $N = 8$, $\alpha_0 = 0°$. (**a**) 3-D view; (**b**) The contour line, read circle is contour line of 0.5%.

Un-center and un-perpendicularity of the current-carrying conductor usually coexist in practical situation. Especially, the effect of the conductor position error will become increasingly difficult to ignore in the situation that the conductor is soft wire, which may be not strictly straight and fixed in a certain position. For that reason, the combination of the relative error, $\varepsilon_{d\beta}$, caused by un-center and un-perpendicularity become more necessary to consider together. In Figure 4, $\varepsilon_{d\beta}$ is calculated by equation (11) with $N = 8$, $r_0 = 40$ mm, it can be seen that the relative errors retain in 0.5% with major region of d and β. With the approximate region of -10 mm$< d <$10 mm and $-30° < \beta < 30°$, the relative errors retain in 0.077%, and increase rapidly as the absolute value of d and β both increasing. For the extreme situation, $\varepsilon_{d\beta}$ come up to 20.25% with $\beta = \pm 60°$, $d = \pm 23$ mm and $N = 8$. Table 2 list the value of $\varepsilon_{d\beta}$ with N ranges from 2 to 16 with different d and β. From the table, extreme $\varepsilon_{d\beta}$ can be reduced to 2.896% through increasing N to 16, and become an ignorable level with the region of -10 mm$< d <$10 mm and $-30° < \beta < 30°$.

Table 2. Theoretical $\varepsilon_{d\beta}$ with N ranges from 2 to 16, $r_0 = 40$ mm.

N	$\varepsilon_{d\beta}$ (%) with $\beta = \pm 60°$, $d = \pm 23$ mm*	$\varepsilon_{d\beta}$ (%) with $\beta = \pm 30°$, $d = \pm 10$ mm
2	198.8	23.17
4	72.48	2.9464
6	36.05	0.4665
8	20.25	0.07696
10	12.04	0.01279
12	7.382	0.002129
14	4.601	0.0003544
16	2.896	0.000005899

** The extreme situation in our case.*

Preprints (www.preprints.org) | NOT PEER-REVIEWED | Posted: 29 January 2018 doi:10.20944/preprints201801.0272.v1

4. Experimental Procedure

The experiment setup is as shown in Figure 5. Four or Eight commercial TMR sensors (TMR2103) were placed on an annular PCB. The circle radius of sensors array was 40 mm. TMR2103 is manufactured by MultiDimension Technology (MDT), with the linear measurement range of ±30 Oe [15] and high sensitivity of 6 mV/V/Oe (1 Oe = 1 Gauss in air = 0.1 millitesla = 79.8 A/m). TMR2103 includes four Magnetic Tunnel Junction (MTJ) elements constructing a Huygens bridge. In comparison with Hall effect sensor, AMR sensor, GMR sensor and other magnetic sensors, TMR sensor has higher sensitivity, better temperature stability, lower power consumption and better linearity [16,17]. Especially, TMR sensor has higher frequency range [18], which is the advantage for higher frequency AC or transient current measurement.

The outputs signal of TMR2103 was detected by a PCI DAQ system of National Instruments (NI PXIe-6366) and processed via the LabVIEW software. The current source (AHY-15-10-200) can provide a stable maximum 200 A current with the frequency range of 40 to 600 Hz. The current in the current-carrying conductor was also measured by current probe TCP0150 with an accuracy of 0.01% and a frequency range of DC to 2 MHz, which could be treated as a reference current sensor in our case. In the purpose to reduce the power noise, the power of sensors array was supplied by a battery through a linear DC stabilizer voltage supply board. The system diagram of the experimental setup was similar to the proposed work by Renzo Bazzocchi *et al* [3], furthermore, we improved that by an adjustable shelf so that the d and β can be adjusted conveniently and accurately. The yellow arrows in Figure 5 represent the equipment is adjustable along the pointed directions. The most components in the setup, including the adjustable shelf, the optical platform are made of non-ferromagnetic materials for insuring the stray magnetic field interference being minimized.

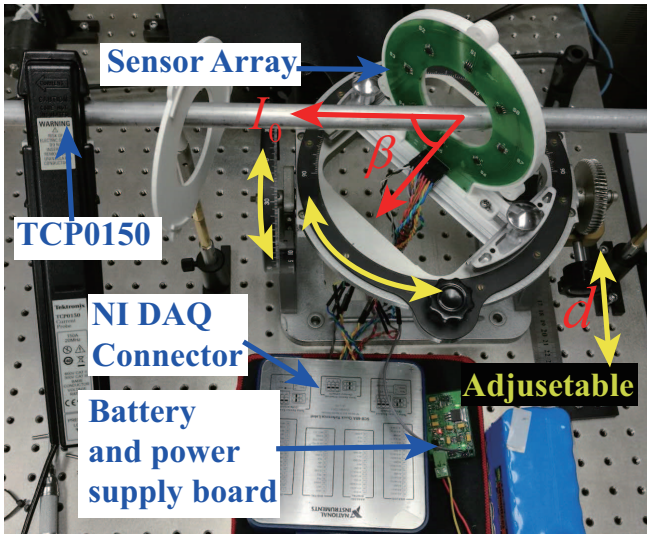

Figure 5. Experiment setup with adjustable platform.

Firstly, the calibration was conducted with five separate measurement cycles with the current from 10 A to 140 A and back, at the frequency of 400 Hz. The output signals of all the sensors in the array and the measurement result of TCP0150 were detected. The root-mean-square (RMS) of the each signal was calculated. And then, the sensors outputs and the reference result from TCP0150 were fit by the linear least-squares method, which were realized in LabVIEW and Matlab. After that, the differences of sensitivity for all TMR sensors could be minimized. In this procedure, the current-carrying conductor were strictly crossing the center of the circle and be perpendicular on the sensors array plane.

Following the calibration, keep $\beta = 0°$, for the d changing from -24 mm to 24 mm with the step of about 5 mm , the multiple RMS measurements of the output signals of TMR sensors array

Preprints (www.preprints.org) | NOT PEER-REVIEWED | Posted: 29 January 2018 doi:10.20944/preprints201801.0272.v1

were conducted. After that the same procedure was conducted for the β changing from -60° to 60°, keeping $d = 0$. Note that, we kept $\alpha_0 = 0$ in all procedures, because only the maximum relative error will be considered about in our analysis.

5. Results

5.1. The calibration result

The calibration for individual sensor had been conducted as presented in the experimental procedure section. In Figure 6, the curves were fit by the linear least-squares method and the results were list. It could be seen that the difference between the eight TMR sensors are obvious, which also exist in other kind of magnetic sensors e.g. GMR sensors, AMR sensors or hall sensors. After fit the individual sensor output characteristics, the parameters were used to calculated every sensor measurement result, so that the differences were minimized effective. That leads the assumption in the mathematical model, that the sensitivities of sensors k_s were equal, being available.

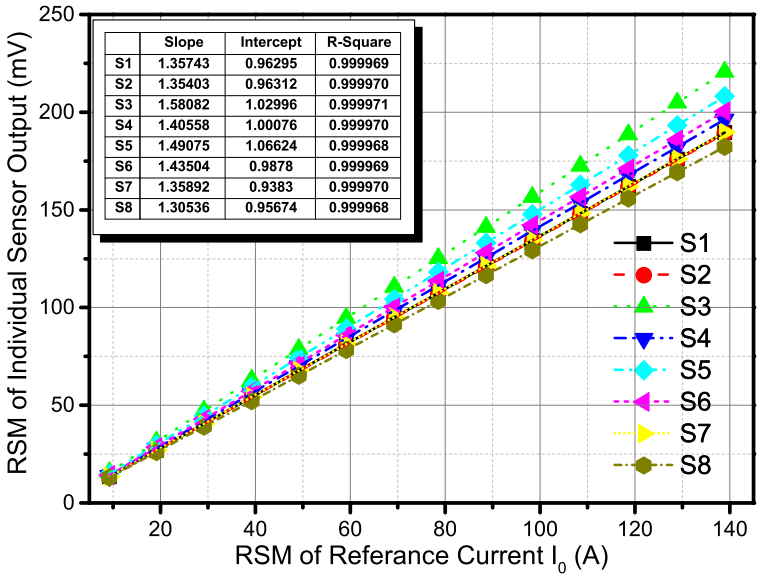

Figure 6. Calibration result for individual output of sensors. The results of linear fit for individual sensor are list in the table.

5.2. The result of un-center and un-perpendicularity

As the procedure proposed in the experimental procedure section, the theoretical and experimental results of the relative error caused by un-center and un-perpendicularity were conducted respectively. For d changing from -24 mm to 24 mm, the result of ε_d was shown in Figure 7(a) with $N = 4$, and in Figure 7(b) with $N = 8$. It could be seen that ε_d achieved the maximum value for $d = \pm 23$ mm and retained in a small value for in the range of -10 mm to 10 mm. The theoretical results was verified by the experimental results with four and eight TMR sensors. The relative error ε_d reduced below 0.2% (for example) by increasing the number of sensor from 4 to 8, with -10 mm$< d <$10 mm. From another perspective, for the purpose of keeping relative error below 0.2% (for example), the allowable range of d will be expended from ± 5 mm to ± 10 mm while increasing the sensors number from 4 to 8.

The relative error caused by un-perpendicular was measured and calculated, as shown Figure 8(a) and Figure 8(b). The proposed theory was also well verified by the experimental results. For different β from -30° to 30°, the relative error caused by β retained in 0.2% with eight TMR sensors.

Preprints (www.preprints.org) | NOT PEER-REVIEWED | Posted: 29 January 2018 doi:10.20944/preprints201801.0272.v1

That is illustrated that, increasing the number of the sensors lead the current measurement by sensors array has more accuracy and reliability.

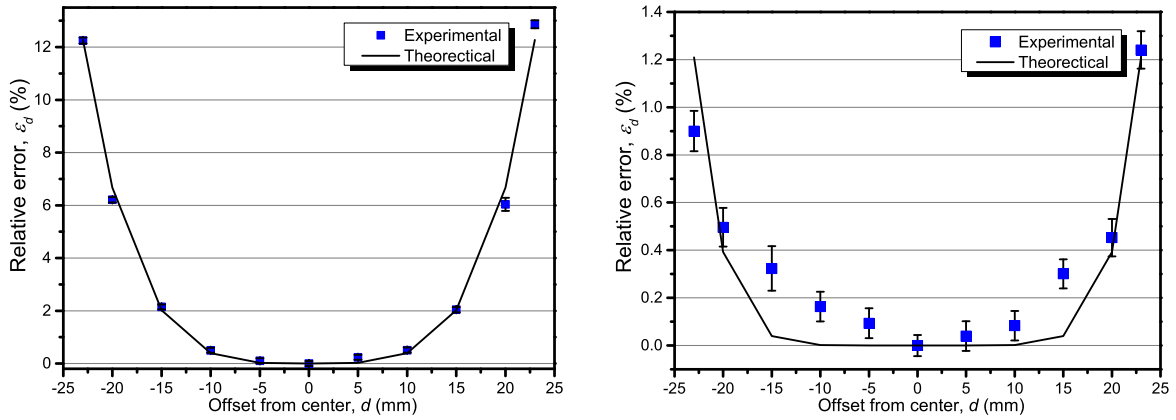

(a) $N = 4$ (b) $N = 8$

Figure 7. The un-centered effect with the offset distance d various from -23 mm to 23 mm, with $\beta = 0°$, $\alpha_0 = 0°$, the test current is f=400 Hz @ 50 A.

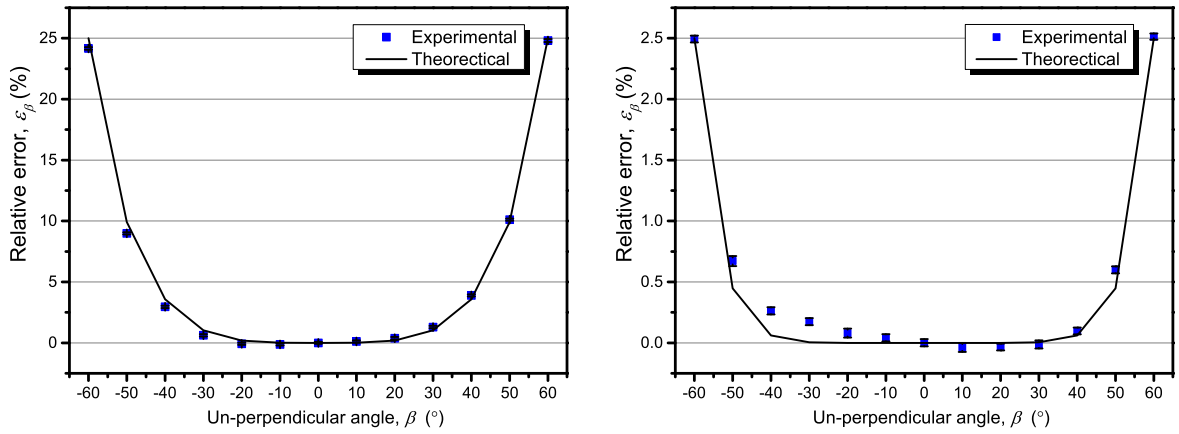

(a) $N = 4$ (b) $N = 8$

Figure 8. the un-perpendicular effect with the offset angle β various from -60° to 60°, with $d = 0$, $\alpha_0 = 0°$, the test current is f=400 Hz @ 50 A.

6. Discussion

However, there still exited errors between the experimental and the theoretical results, which might be caused by these factors: Position error of the experiment setup especially the adjustable shelf. The experimental setup can be improved by the high precision electromotional translation stage which has multiple degrees of freedom; The residual calibration error of individual TMR sensor; The sensitivity axis error of TMR sensors (might not be strictly perpendicular to r_0).

In spite that, the experimental and the theoretical results in this paper can be a reference to design the circular array of TMR sensors for current measurement in practical cases. From the equation (11), the effect of the un-center offset d, the un-perpendicular angle β, the number of TMR sensor N and the radius of the circle r_0 are obvious. At the same time, the linear range of TMR sensor and the maximum under measured current limit the radius of the circle by equation (1). In the purpose to reducing the relative error $\varepsilon_{d\beta}$, the un-center offset d and un-perpendicular angle β can be limited by mechanical

 doi:10.20944/preprints201801.0272.v1

structure design. For instance, it is can minimize the gap between the current-carrying conductor and the shell of the sensors array to limit the offset d. It is also can limit the un-perpendicular angle β effectively by increasing the thickness of the shell of sensors array along the direction of z-axis.

Furthermore, the relative error $\varepsilon_{d\beta}$ can be reduced below usual level that can be neglected, by increasing the number of magnetic sensors to 16 or more by the calculated result of (11). It is necessary to have a tradeoff between the accuracy and the cost in an actual case. Although the analysis has been presented in the case of several conditions, however, there are also many factors, that may cause measurement error, has not discussed in this paper. For instance, the crosstalk current interference, the earth magnetic interference, .etc. For individual TMR sensor, its hysteresis [19–22] , nonlinearity, bandwidth, temperature property, etc. can not be neglected. In the application of the circular array of TMR sensors, the signal process circuit must be designed well to calibrate the individual sensor and output the sum of all the sensors. For the reason that the approach proposed in this paper has the ability to measure DC to high frequency current, the further work will focus on the AC frequency response test and the extension for the frequency bandwidth of the circular array of magnetic sensors.

7. Conclusion

We analyzed the relative measurement error of circular array of magnetic sensors caused by position error of the current-carrying conductor in this paper. The theoretical results were proposed and verified by the actual experiment setup. The effect on relative error caused by un-center offset, un-perpendicular angle, number of magnetic sensor and the radius of the circle are expressed in one equation. The allowable range of un-center offset and un-perpendicular angle are give to insure the relative error retaining in acceptable level.

Acknowledgments: This work is supported by the National Natural Science foundation of China (No. 61573046), and is also supported by the Program for Changjiang Scholars and Innovative Research in University (No. IRT1203).

Author Contributions: H.Y. and Z.Q. conceived and designed the experiments; J.Q. performed the experiments; H.L. and H.Y. analyzed the data; H.Y. wrote the paper.

Conflicts of Interest: The authors declare no conflict of interest.

Abbreviations

The following abbreviations are used in this manuscript:

AMR	Anisotropic Magnetoresistance
GMR	Giant Magnetoresistance
TMR	Tunnel Magnetoresistance
MTJ	Magnetic Tunnel Junction
AC	Alternation current
DC	Direct current
RSM	Root mean square

Bibliography

1. Ennen, I.; Kappe, D.; Rempel, T.; Glenske, C.; Hütten, A. Giant Magnetoresistance: Basic Concepts, Microstructure, Magnetic Interactions and Applications. *Sensors* **2016**, *16*, 904.
2. Ripka, P.; Kejik, P.; Kaspar, P.; Draxler, K. Precise DC current sensors. IEEE Instrumentation and Measurement Technology Conference, 1996, Vol. 2, pp. 1479–1483 vol.2.
3. Bazzocchi, R.; Di Rienzo, L. Interference rejection algorithm for current measurement using magnetic sensor arrays. *SENSORS AND ACTUATORS A-PHYSICAL* **2000**, *85*, 38–41.
4. Rienzo, L.D.; Bazzocchi, R.; Manara, A. Circular arrays of magnetic sensors for current measurement. *IEEE Transactions on Instrumentation and Measurement* **2001**, *50*, 1093–1096.
5. Mlejnek, P.; Vopálenský, M.; Ripka, P. AMR current measurement device. *Sensors & Actuators A Physical* **2008**, *141*, 649–653.

6. Weiss, R.; Makuch, R.; Itzke, A.; Weigel, R. Crosstalk in Circular Arrays of Magnetic Sensors for Current Measurement. *IEEE Transactions on Industrial Electronics* **2017**, *64*, 4903–4909.
7. Weiss, R.; Itzke, A.; Weigel, R. Current measurement of flat conductors with a circular array of magnetic sensors. 2017 IEEE Second International Conference on DC Microgrids (ICDCM), 2017, pp. 166–170.
8. Guo, Q.; Fu, P.; Gao, G.; Jiang, L.; Wang, L.S.; Bai, Y.R. Rectangular Magnetic Sensor Array for Current Measurement by the Quadrature Method. *IEEE Transactions on Plasma Science* **2017**, *PP*, 1–7.
9. Ziegler, S.; Woodward, R.C.; Iu, H.H.C.; Borle, L.J. Current Sensing Techniques: A Review. *IEEE Sensors Journal* **2009**, *9*, 354–376.
10. Wisniowski, P.; Wrona, J.; Stobiecki, T.; Cardoso, S.; Freitas, P.P. Magnetic Tunnel Junctions Based on Out-of-Plane Anisotropy Free and In-Plane Pinned Layer Structures for Magnetic Field Sensors. *IEEE Transactions on Magnetics* **2012**, *48*, 3840–3842.
11. Dabek, M.; Wisniowski, P. Dynamic response of tunneling magnetoresistance sensors to nanosecond current step. *Sensors & Actuators A Physical* **2015**, *232*, 148–150.
12. Dabek, M.; Wisniowski, P.; Stobiecki, T.; Wrona, J.; Cardoso, S.; Freitas, P.P. Sensitivity and 3 dB Bandwidth in Single and Series-Connected Tunneling Magnetoresistive Sensors. *Sensors* **2016**, *16*.
13. Liu, Y.; Xie, X.; Hu, Y.; Qian, Y.; Sheng, G.; Jiang, X. A Novel Transient Fault Current Sensor Based on the PCB Rogowski Coil for Overhead Transmission Lines. *Sensors* **2016**, *16*.
14. Berendsen, H.J.C. *The Cambridge Handbook of Physics Formulas*; 2007.
15. MDT. TMR2103 Tunneling MagnetoResistance sensor.
16. Lenz, J.; Edelstein, A.S. Magnetic sensors and their applications. *IEEE Sensors Journal* **2006**, *6*, 631–649.
17. Ouyang, Y.; He, J.; Hu, J.; Zhao, G.; Wang, Z.; Wang, S.X. Prediction and Optimization of Linearity of MTJ Magnetic Sensors Based on Single-Domain Model. *IEEE Transactions on Magnetics* **2015**, *51*, 1–4.
18. Ouyang, Y.; Hu, J.; He, J.; Zhao, G.; Xue, F.; Wang, Z.; Wang, S.X.; Yuan, Z.; Ding, Z. Modeling the Frequency Dependence of Packaged Linear Magnetoresisitive Sensors Based on MTJ. *IEEE Transactions on Magnetics* **2014**, *50*, 1–4.
19. Xiaodong, Z.; Zheng, Q.; Yuan, T.; Jingyi, W.; Hao, Y. The error compensation for static hysteresis characteristics of Giant Magneto-Resistance sensor. 2016 IEEE Sensors Applications Symposium (SAS), 2016, pp. 1–5.
20. Xiaodong, Z.; Zheng, Q.; Kaikai, P. The Analysis of Hysteresis in the Spin Valve Magneto-resistance. 2013 Third International Conference on Instrumentation, Measurement, Computer, Communication and Control, 2013, pp. 736–739.
21. Jedlicska, I.; Weiss, R.; Weigel, R. Linearizing the Output Characteristic of GMR Current Sensors Through Hysteresis Modeling. *IEEE Transactions on Industrial Electronics* **2010**, *57*, 1728–1734.
22. Xie, F.; Weiss, R.; Weigel, R. Hysteresis Compensation Based on Controlled Current Pulses for Magnetoresistive Sensors. *IEEE Transactions on Industrial Electronics* **2015**, *62*, 7804–7809.